A Correlation Study of Averaged and Single Trial MEG Signals: The Average Describes Multiple Histories Each in a Different Set of Single Trials

Lichan Liu* and Andreas A. Ioannides*^

Summary: Our understanding of the link between electrical events in the brain and behaviour is based on indirect measures. Positron Emission Tomography (PET) and functional Magnetic Resonance Imaging (fMRI) rely on haemodynamic processes which are slower by two to three orders of magnitude than the processes characterizing normal and pathological brain function. Direct invasive measurements of the electrical activity on the other hand produce too local a view which fails to show the large scale coherence which sustains awareness and cognition. On the opposite extreme, gross measures of the electrical activity like Electroencephalography (EEG) and single or few channel Magetoencephalography (MEG) had until recently to rely on simplistic point like models extracted from the averages of many repetitions of physiologically irrelevant stimuli. The introduction of multichannel probes with over 30 channels (Hämälainen et al. 1993), and the use of distributed source analysis (Ioannides et al. 1990a) opened up for the first time the possibility to study the response of single trials. In this work we address directly the question how representative is the description of events extracted from the analysis of the average signal. We use the simplest possible example: the cortical response to a simple 1 kHz tone, focusing on the early and by general admission "automatic" response around 100 ms after stimulus onset. To avoid the confounding inter-subject variability we have studied the responses over the left and right cortical areas to ipsi- and contralateral stimulation in a single subject; for testing reproducibility, we have used both the eyes open and eyes closed conditions. Since the computational demands involved in extracting a full three dimensional description from each trial are too great,we have complemented the distributed source analysis with special techniques, which allow us to scan through each and every single trial and identify each cortical activation similar to the ones picked out in the average signal. We are thus able to show conclusively that the sequence of events suggested by the analysis of the average signal is not representative of what is happening in individual trials. The sequence is made up of events which occurred in different trials reflecting probably the existence of many parallel routes each of which leads from the input at the ear to a final "computation".

Key words: Human auditory evoked fields; Magnetoencephalography (MEG); 40-Hz Oscillation; Single epoch analysis; Vector signal transformation V_3; Spatiotemporal correlation measures.

Introduction

Understanding brain function requires information about single neuron activity and activity involving many thousands of neurons behaving in a temporally organised way. At the single neuron level, experiments designed to test the specificity of response to a stimulus do indeed demonstrate such specificity in a remarkable degree (Hubel and Wiesel 1962; Desimone et al. 1984; O'Keefe and Recce 1993). Other experiments and modelling studies show that the activity of individual neurons and their membership to neuronal populations associated with a specific task can be highly variable (Vaadia et al. 1995). Furthermore, evidence has been accumulating slowly but steadily over the years, for correlates of behaviour which involve synchronous mass population activity (Nicolelis et al. 1995) and sparse coding (Mitzdorf et al. 1994).

Progress in neuroscience depends on integrating the information generated by the ever more complex techniques and analysis methods, covering widely different temporal and spatial scales, and reconciling the seemingly contradictory conclusions that one obtains from a first interpretation of the results of each methodology. Much effort has recently been directed to the combination of haemodynamic and electrographic techniques, because the first produces accurate positional information, while the latter has the required temporal resolution. In pooling this information, it is necessary to be aware of the mechanisms involved and take a fresh look at the as-

*Department of Physics, The Open University, Milton Keynes, U.K.
^Institute of Medicine, Research Centre Jülich, Jülich, Germany.

The methodology and computer tools were developed, and the early applications performed, as partial fulfillment of the requirements for the Ph.D degree by L.C. Liu, supported by a studentship from the Department of Physics, The Open University, U.K.

Further support from the Leverhulme trust is also acknowledged.

Correspondence and reprint requests should be addresed to A. A. Ioannides, Institute of Medicine, Research Centre Jülich, D-52425 Jülich, Germany.

Fax: 49 (0)2461 612820

E-mail: andy@imemeg1.ime.kfa-juelich.de

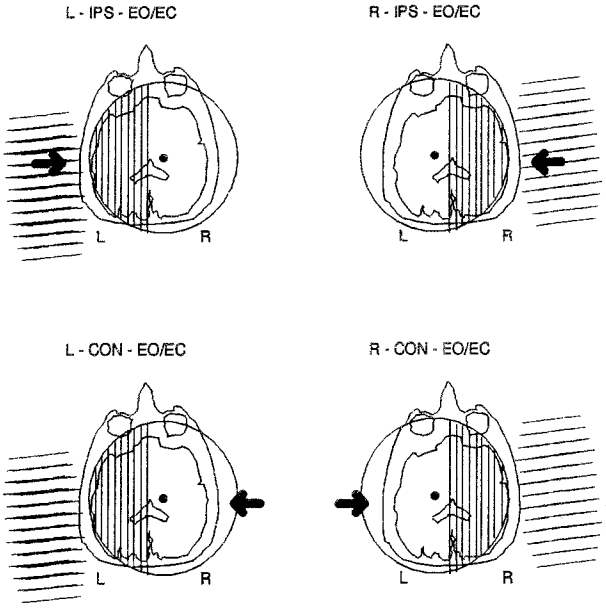

Figure 1. Experiment set-ups in an axial view: each sensor is represented by a line along its baseline, and the side where the stimulus is delivered is marked by the heavy arrow. The source space used to confine the primary current density in the MFT analysis is a spherical segment which for display purposes is sectioned into 9 cuts (tomes), as shown in each diagram. For each case, the outline of the sphere used to define the source space is also drawn with its centre coinciding with the centre of the conducting sphere, which is marked by a heavy dot.

sumptions and idiosyncrasies introduced to the analysis in each method by its history. The work we will report points to deficiencies in the conventional analysis of bioelectromagnetic signals. We will particularly point out why extreme care must be taken in interpreting the numerous recent studies which combine positional information from PET and fMRI with temporal information extracted from average Electroencephalographic (EEG) and/or Magnetoencephalographic (MEG) signals.

Traditional methods of analysis of bioelectro-magnetic signals (EEG and/or MEG) have relied on averaging a large number of responses from identical and well defined (in terms of physical properties) stimuli, but with little or no biological significance. The problem of how such a method can be justified when one knows that there is substantial trial to trial variability was acknowledged (Basar et al. 1989; Haig et al. 1995; Lütkenhöner et al. 1995), but largely ignored in the overriding need to eliminate what was considered to be background (mainly biological) noise. The recent advent of multi-channel MEG systems make it possible to record brain activity in real time over a large area of the head; it is perfectly feasible to extract reliable estimates of brain activity, at least over the cortical mantle below the sensors, from single trial signals (Ioannides 1994a). Simple signal transformations and correlation measures which are based on these transformations make feasible for the first time the detection of specific cortical activation in each and every single trial (Liu 1995).

We have used auditory evoked MEG signals from an experiment consisting of eight distinct cases (Singh et al. 1994). For all eight cases the average signal was computed, and for seven out of eight cases (the raw signal for one case could not be used) 125 single trial signals were extracted from 500 ms before to 500 ms after the onset of the stimulus. We have chosen this very standard experiment to study in detail how the strong cortical activations observed in the average are reflected in each single trial. To achieve this we have used Magnetic Field Tomography (MFT) (Ioannides 1994a) and a simple vector signal transformation called $\mathbf{V}_3$ which highlights nearby sources (Liu and Ioannides 1995). MFT has been applied to the average MEG signals and some single trial records; the resulting estimates of millisecond by millisecond brain activity were superimposed with co-registered MRI images of the background anatomy in both static images (Singh et al. 1994) and animations (Ioannides 1993). MFT is however computationally demanding and the follow up inspection of huge number of three-dimensional images makes it impracticable to apply to each and every single trial, despite the availability of a dedicated 30 node transputer system (Liu et al. 1993). By constructing correlation estimators based on the $\mathbf{V}_3$ over a finite time interval and areas of interest, we were able to scan through all single trial data and extract reliable measures about how each single trial compares with the average (Liu 1995). We will report our findings for the single trial manifestation of the M100 component, which dominates the average signal, and the next strong component at about 135 ms. We also compare the 40-Hz signal component in the average signal and single trials for the same experiment, and we will use the results to comment on recent apparently contradictory conclusions about the significance of 40-Hz activity.

Methods

Experimental set-up

We have used a set of auditory evoked measurements obtained with the KRENIKON 37 channel system (Singh et al. 1994). The experiment was carried out to measure the ipsilateral and contralateral response of the left and right hemisphere when an auditory stimulus (a 600 ms long, 1kHz auditory tone) was applied monaurally to the left or right ear, and separately for each case for the eyes open or closed condition (8 cases in total, see figure 1). The subject was a normal right-handed 26 year-old male and in this experiment was asked to stay alert but not to pay attention to any particular feature of the stimulus. A three-label

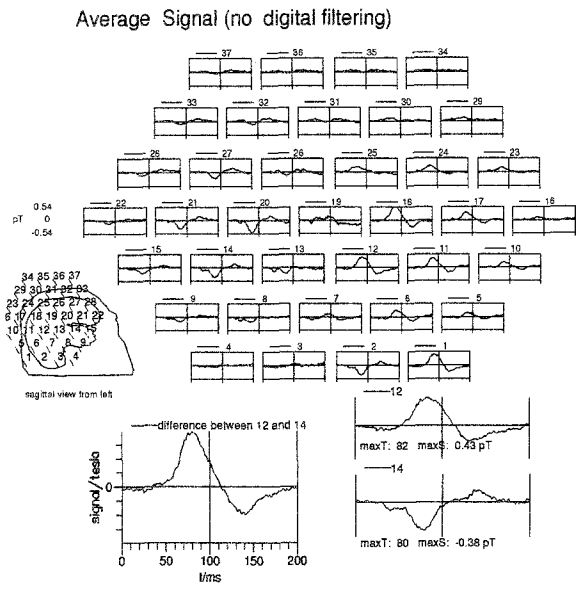

Figure 2. Case L-CON-EC: the average signal for the 37 MEG channels without digital filtering. The sketch of the head shows the relative position of the channels in relation to the head. The lower right part of the diagram shows the signals for channels 12 and 14, which have very similar high magnitude but opposite phase to each other; the difference mimicking the effect of $\mathbf{V}_3$ at channel 13 (between channels 12 and 14) is displayed on the left.

binary code was used to classify the 8 cases: the first index defines which temporal area the dewar was over, left (L) or right (R); the second index denotes the side which the simulation was used, ipsilateral (IPS) or contralateral (CON) side in relation to the dewar; and finally the third index specifies whether the eyes were open (EO) or closed (EC). For example, case L-CON-EC means that the dewar was over the left temporal area, the stimulus was delivered to the right ear and the eyes were closed.

MFT Analysis

MFT uses probabilistic estimates for the (non-silent) primary current density vector $\mathbf{J}^p(\mathbf{r},t)$ at each timeslice of signals (Ioannides et al. 1990a). The logical and algorithmic steps of MFT are described elsewhere (Ioannides 1994b) as is the way MFT has broken away from the historical link with EEG methodology, which has slowed down the development of MEG analysis (Ioannides et al. 1994a).

The original signal and the current density $\mathbf{J}^p(\mathbf{r},t)$ have positive and negative components, while the intensity $P(\mathbf{r},t)$ ($P(\mathbf{r},t)=\mathbf{J}^p(\mathbf{r},t)\cdot\mathbf{J}^p(\mathbf{r},t)$) is a positive scalar. Hence operations like summation and subtraction can be performed on $P(\mathbf{r},t)$ without the huge cancellations which occur when the same operations are applied to the signals or $J(\mathbf{r},t)$. Furthermore, $P(\mathbf{r},t)$ can be used in integrals over space and/or time, to provide hints of how the brain activity changes over a specific area, i.e., region of interest (ROI), and/or a longer period Δt (Ioannides 1994b; Ioannides et al. 1995b). We give for completeness the expressions for the integrals over space $A(t, \Delta t)$ and time $I(\mathbf{r}, t, \Delta t)$, which are routinely used in MFT analysis:

$$I(\mathbf{r},t,\Delta t)=\int_{t-\frac{\Delta t}{2}}^{t+\frac{\Delta t}{2}} P(\mathbf{r},t')dt' \qquad (1)$$

$$A(t,\Delta t)=\int_{t-\frac{\Delta t}{2}}^{t+\frac{\Delta t}{2}} dt' \int_{ROI} P(\mathbf{r},t')d^3\mathbf{r} \qquad (2)$$

The first integral can be thought of as an image which as the Δt integration period becomes very large it can be contrasted, but not identified (Ioannides 1995a), with corresponding fMRI or PET images. The second integral provides a measure of the time course of activity emanating from a region which can be fairly small (a fraction of a centimeter across for superficial generators) or a large area. These measures are of course blind to the silent part of the source, i.e., any current flows which produce no external magnetic field.

$\mathbf{V}_3$ Analysis

The full MFT computation is very time consuming, making it extremely difficult to process large amounts of data. Inspecting the signal traces directly is hard because the relationship between the generators and the radial component of the magnetic field they generate is not simple: in fact directly above a superficial generator the radial component of the magnetic field is zero. The MEG signal need not be so unintelligible: a solution can be found in hardware, e.g., by measuring a tangential field component or the field derivative which is maximum above a superficial generator. The first option is usually avoided because it leads to a dependence on return currents which complicates the analysis, while the second is likely to improve sensitivity to nearby superficial sources at the expense of sensitivity to deep generators. The Helsinki group have pioneered the hardware implementation of radial derivatives, and this is the option used in the current 128 channel NEUROMAG helmet system (Ahonen et al. 1992). A software solution can however be defined which has an identical effect, and it preserves the sensitivity of the original measurements to deep sources. The idea is simply demonstrated in figure 2, which shows the average signal in case L-CON-EC without any digital filtering for the first 200 ms after the onset of the stimulus. The figure also provides a plan view of the sensor arrangement and the relative orientation with respect to the head. The signal is consistent with a strong focal source, roughly below channels 13 and

19, because the signals in these channels mark a transition between the neighbouring channels on either side (e.g., channels 12 and 14, 18 and 20), which have large signals of opposite polarity. Channels 13 and 19 registered a very weak signal and hence are inappropriate as markers for nearby sources (the zero level crossing can be easily shifted if another generator is some distance away). The difference between channels 12 and 14 approximates the derivative at channel 13, and it is a strong signal (see the insert in the bottom left of figure 2), which is robust because it is not changed much by contributions from other more distant generators.

The appropriate operator was first described by Hosaka and Cohen (Hosaka and Cohen 1976) who applied it to cardiac biomagnetic data. The same operator was identified by Ioannides some years later (Ioannides 1987; Ioannides et al.1990b) in a systematic search to improve the intelligibility of the signal. Working through an orderly sequence of irreducible tensor representations of the measurements, the third vector operator had the required properties and it was called accordingly $\mathbf{V}_3$. The $\mathbf{V}_3$ operator has the following properties: it is a model independent transformation depending solely on the experimental geometry; the contribution to the transformed signal from a single localized superficial source exhibits a pronounced feature in the neighbourhood of this source; it decays rapidly as it moves away from a (superficial) generator; the vector properties of the source are reflected in the transformed signal.

The $\mathbf{V}_3$ operator was originally designed as an unbiased estimator for focal as well as extended sources, which highlights the nearby dominant contributions to the MEG signal. It was first used to obtain an initial two-dimensional estimate for a DC current flow in the human leg (Grimes et al. 1985); this estimate was used as the starting configuration in an iterative procedure leading to a three-dimensional line-current source configuration(Grimes and Ioannides 1988). For measurements of the z-component of the magnetic field, S_z , using a planar system, e.g., the KRENIKON 37 channel system, $\mathbf{V}_3(x,y)$ is defined as

$$\mathbf{V}_3(x,y) = \nabla(S_z) \times \hat{\mathbf{e}}_z \tag{3}$$

A spatial smoothing operation is also applied to limit the high sensitivity of derivatives to noise (Liu 1995; Ioannides et al. 1990b):

$$\mathbf{V}_3(x,y,\tau) = \frac{1}{4\pi\tau} \int dy' \int dx' \, e^{-\frac{x'^2+y'^2}{4\tau}} \mathbf{V}_3(x-x', y-y') \tag{4}$$

For a given arrangement of sensors a fixed distribution of (smoothed) $\mathbf{V}_3$ can be approximated by a weighted linear sum of the signal values. Hence, for a fixed set of points and fixed sensor locations, all computationally demanding operations can be done once, allowing the computation of a large number of timeslices (typically 1000 × number of trials × number of conditions) to be performed very fast (Liu 1995).

Comparisons of momentary $\mathbf{V}_3$ distributions are more reliable than comparing the signal itself, but still unsafe. Comparing the spatially smoothed $\mathbf{V}_3$ distributions across finite spatial and temporal domains produces a robust measure. We define the overlap of two $\mathbf{V}_3$ segments of equal length, each defined over the same area A in the measurement plane (i.e., xy plane), one from epoch i (from $t_1 - \frac{\Delta t}{2}$ to $t_1 + \frac{\Delta t}{2}$) and the other from epoch j (from $t_2 - \frac{\Delta t}{2}$ to $t_2 + \frac{\Delta t}{2}$) as follows,

$$\langle i{:}t_1 | A, \Delta t | j{:}t_2 \rangle = \int_A dx\, dy \int_{-\frac{\Delta t}{2}}^{\frac{\Delta t}{2}} dt \, \mathbf{V}_3^i(x,y;t_1+t) \cdot \mathbf{V}_3^j(x,y;t_2+t) \tag{5}$$

Since the $\mathbf{V}_3$ transformation acquires high values whenever a strong superficial generator is present, the overlap provides a similarity measure of superficial activity directly below area A in the measurement plane between the two segments. A measure of similarity which is independent of the magnitude is provided by the normalized correlation coefficient:

$$C_1^{ij}(t_1,t_2) = \frac{\langle i{:}t_1 | A, \Delta t | j{:}t_2 \rangle}{\sqrt{\left|\langle i{:}t_1 | A, \Delta t | i{:}t_1 \rangle\right| \left|\langle j{:}t_2 | A, \Delta t | j{:}t_2 \rangle\right|}} \tag{6}$$

Even with this simplified analysis a comparison of single epochs with each other is prohibitively long. The average response provides an obvious comparison target. First MFT is used to identify strong superficial activity and then a $\mathbf{V}_3$ template for the event is constructed for the average signal. The normalized similarity measure between the average and epoch i is:

$$C_2^i(t_1,t_2) = \frac{\langle aver{:}t_1 | A, \Delta t | i{:}t_2 \rangle}{\sqrt{\left|\langle aver{:}t_1 | A, \Delta t | aver{:}t_1 \rangle\right| \left|\langle i{:}t_2 | A, \Delta t | i{:}t_2 \rangle\right|}} \tag{7}$$

It is advantageous to maintain in the similarity measure the relative magnitude of the single trials which match the average in comparison with the average itself. This is provided by the second correlation measure:

$$C_2^i(t_1,t_2) = \frac{\langle aver{:}t_1 | A, \Delta t | i{:}t_2 \rangle}{\left|\langle aver{:}t_1 | A, \Delta t | aver{:}t_1 \rangle\right|} \tag{8}$$

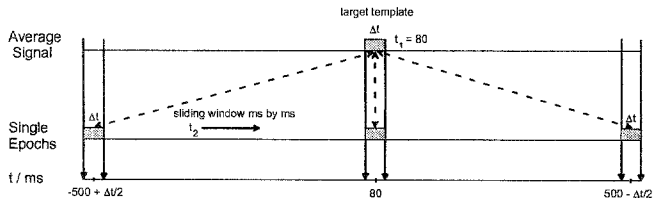

Figure 3. The template of length Δt, centered at t_1 in the average (top) is matched with corresponding template of the same length Δt, centered at t_2 in the ith single trial record, and the correlation $C_1^i(t_1,t_2)$ or $C_2^i(t_1,t_2)$ is computed. The process is repeated by sliding time the single trial template in time, to provide a quantitative measure of how often and strongly the pattern selected in the average is encountered in the single trial record, at different times in relation to the stimulus onset.

Figure 3 shows schematically the scanning through single trials with the target template selected from the average signal; the similarity measures (C_1 and C_2) are computed between the target template and the transformed $\mathbf{V}_3$ signal over the same region and for each segment of the same length in each single trial. For all cases considered in this paper the similarity measures are computed with the target template in the average signal from $t_1 - \frac{\Delta t}{2}$ to $t_1 + \frac{\Delta t}{2}$, and the template of the single trials (1 second long signals, 500 ms on either side of the onset of the stimulus) sliding from $-500 + \frac{\Delta t}{2}$ to $500 - \frac{\Delta t}{2}$ ms.

Results

Comparison of MFT and $\mathbf{V}_3$

At the M100 peak the MFT estimate is focal and superficial. In the lower half of figure 4 an arrow is used to mark the maximum of the current density vector at the most superficial slice of the MFT source space at the latency of the prominent M100 peak. In the top part of the figure the maximum of the $\mathbf{V}_3$ is computed (in the plane of the sensors) and projected onto the cortical surface. The respective maxima are displayed for left and right ear stimulation, and for each case separate figures show the ipsi- and contra-lateral MFT and $\mathbf{V}_3$ maxima.

Average and Single Trial Correlation for M100 and M135

In order to investigate how the M100 pattern extracted from the average is represented in the single trials, we have used the average signal at t_1=80 ms as the target template (see figure 3). During this period, the area of the strongest $\mathbf{V}_3$ corresponded to sensors placed above the

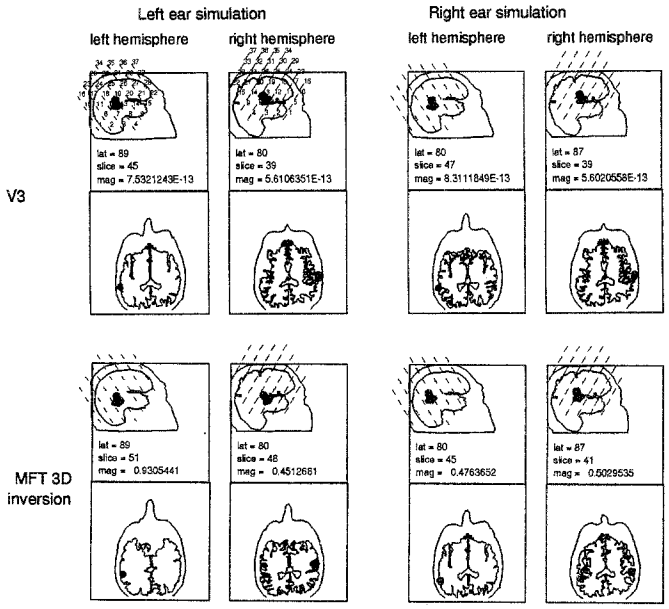

Figure 4. The instantaneous MFT estimate for the M100 is compared with the instantaneous projection of the $\mathbf{V}_3$ estimate onto the cortical surface for all the cases with the eyes open. For each case, the arrow represents the location and direction of the maximum value of the respective MFT or $\mathbf{V}_3$ distribution. Each comparison is done in a fixed sagittal plane through the auditory cortex and in the axial plane closest to the maximum of the MFT or $\mathbf{V}_3$. The axial slice number (*slice*) is printed, and successive axial MRI slices are separated by 1.563 mm. The mismatch of *slice* between MFT and $\mathbf{V}_3$ maximum is of the order of grid separation in the MFT display, which is about 1 cm. In each window, the latency *lat* (ms) and the modulus *mag* of the computed $\mathbf{V}_3$ and MFT are also printed. The units for the $\mathbf{V}_3$ are *T/m* while for MFT are arbitrary.

posterior end of the Sylvian fissure. For each epoch, $C_1(80,t)$ and $C_2(80,t)$ were computed for 1000 - Δt ms (from $-500 + \frac{\Delta t}{2}$ to $500 - \frac{\Delta t}{2}$ ms, see figure 3). Figure 5 shows the total number of single trials, for case L-CON-EC, having $C_1(80,t)$ and $C_2(80,t)$ above the threshold as a function of time (0 to 200 ms after the onset of the stimulus), for template lengths of Δt = 0, 10, 20 and 40 ms respectively. The figure demonstrates that for the M100, which has a relatively long and stable activation pattern from 60 to 100 ms, varying the template length Δt changes little the correlation coefficients. However, when the template target is moved to other peaks of the average signal, care must be taken to choose an optimal template length in order to reflect the simultaneity and pattern of the brain activity over a short period. The correlation analysis was also applied to all single trials with the target template in the average around 135 ms (i.e., t_1=135 ms) and the template length of 10 ms (i.e., Δt=10 ms). In the following

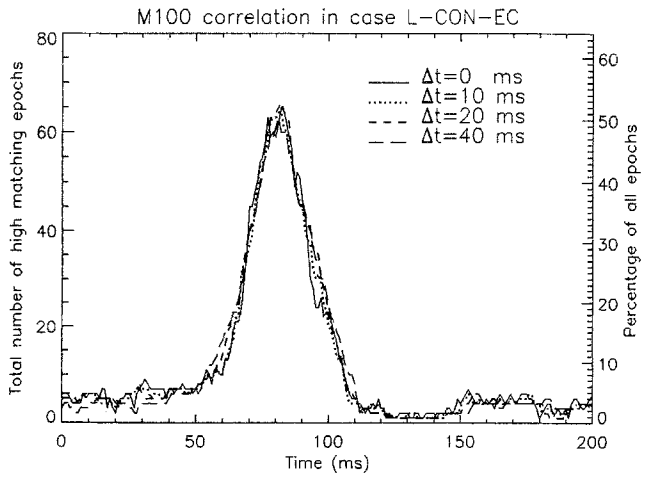

Figure 5. The effect of different template lengths Δt on the correlation coefficients $C_1(80,t)$ and $C_2(80,t)$ in case L-CON-EC. The total number of epochs having ($C_1 \geq 0.6$ and $C_2 \geq 1.0$) is plotted as a function of time, for template lengths $\Delta t = 0$, 10, 20 and 40 ms, respectively.

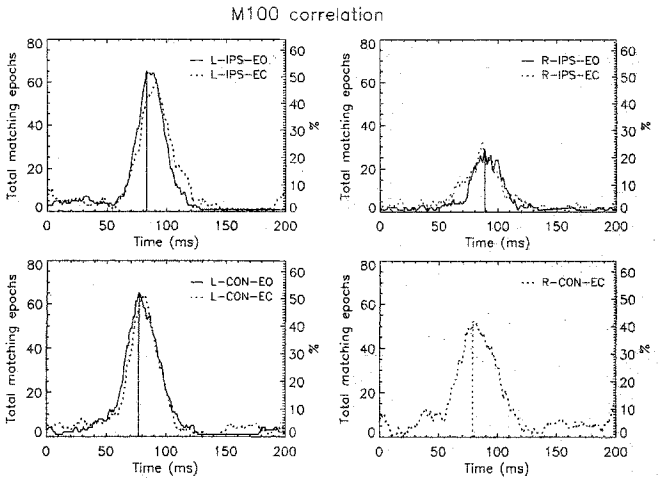

Figure 6. The total number of high matching epochs with the M100 seen in the average in all 7 cases from 0 to 200 ms: The left vertical axis indicates the total number of the high matching epochs, while the right vertical axis is the corresponding percentage in all the epochs. The solid and dotted lines stand for the eyes open and closed condition, respectively. The latency where the number of matching epochs reaches its maximum, for the eyes open condition, is marked by a solid vertical line.

discussion of the M100 correlation, we choose Δt=10 ms as the template length.

Figure 6 shows the correlation between the average and single trials for the M100 during the first 200 ms after the onset of the stimulus. In all 7 cases, one or more single trials could be found that matched the M100 pattern seen in the average for any one latency selected. The number of matching epochs however increases dramatically around the M100, i.e., at around 77-91 ms, the total number of high matching epochs reaches the peak. For the cases when the probe was placed over the left hemisphere, about 60-65 epochs out of 125 epochs (48%-52% of all epochs) have high matching at the peak latency. In agreement with earlier studies based solely on the average signals (Liu 1995; Singh et al. 1994), we also find that the M100 peak is reached earlier in single epochs when the stimulus was from the contralateral side than that from ipsilateral side. Note, however, the qualitatively different interpretation of our single trial analysis: for each condition the M100 onset is described by a distribution of the high matching trials with the average in time, with shifts in latency of the maximum of matching trials being consistent with the shifts in the peak latency when the average signal for each condition is analysed.

Figure 7 shows the M135 correlation for the eye closed condition (4 cases) superimposed onto the M100 correlation. At around the M135 peak (131-154 ms), the number of epochs matching the M135 target template in the average reaches the peak in all cases. The left hemisphere has higher number of epochs (39-44 epochs, 31%-35% of all epochs) than the right hemisphere (16-24

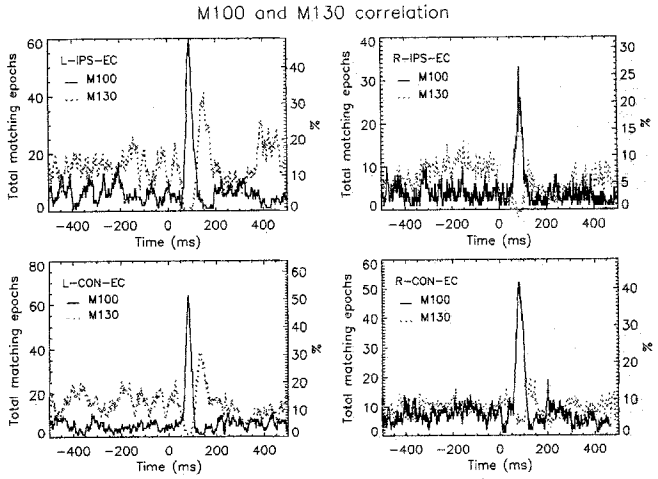

Figure 7. The total number of high matching epochs for the M100 (solid) and M135 (dotted) for the 4 cases with the eyes closed from -500 to 500 ms.

epochs, 13%-19% of all epochs). At the M100 peak, the total number of the epochs having the M135 is at minimum, while at the M135 peak, the epochs having high M100 correlation is at minimum.

Tables 1 and 2 show the total number of epochs matching the average templates at around M100 and M135, respectively. The tables also contain information about how many epochs match one or other template

Table I. A summary table for all the available single trial data (7 out of 8 cases) in the M100 correlation. The first column identifies the case, and the second column shows the average number of trials ($\bar{n}$) having high M100 correlation ($C_1 \geq 0.6$ and $C_2 \geq 1.0$) during the 500 ms long pre-stimulus interval. The next three columns summarize the M100 correlation during the M100 peak period (from 77 to 91 ms): the average number of trials having high M100 correlation ($\bar{n}_1$), the latency where the number of high matching trials is maximum (T_1) and the maximum number of high matching trials (N_1), which are spilt into trials which have high M100 matching only and trials which have both high M100 and M135 matchings, as stated by the numbers in the bracket. Column 6 shows the total number of epochs (S_1), and in bracket the corresponding percentage, which, for at least one latency between 60 and 100 ms, match the M100 average. Columns 7 to 9 summarize the M100 correlation during the M135 peak period (from 131 to 154 ms): the average number of high matching trials ($\bar{n}_2$), the latency where the M135 correlation is at peak (t_2) and the number of high matching trials (n_2) at the latency of (t_2).

case label	pre-stm.	M100 period				M135 period		
	$\bar{n}$	$\bar{n}_1$	T_1(ms)	N_1(o./b.)	S_1(%)	$\bar{n}_2$	t_2(ms)	n_2
L-IPS-EO	3.0	58.7	83	65(42/23)	83(66)	0.5	144	0
L-IPS-EC	6.3	49.7	91	60(38/22)	79(63)	3.1	154	2
L-CON-EO	3.8	54.5	77	65(44/21)	87(70)	0.7	140	1
L-CON-EC	5.1	55.8	81	64(45/19)	82(66)	2.0	135	1
R-IPS-EO	2.1	22.4	89	29(27/2)	69(55)	0.4	146	0
R-IPS-EC	1.4	25.3	87	33(24/9)	79(63)	0	131	1
R-CON-EC	7.7	47.7	79	52(44/8)	83(66)	4.8	133	2

Table II. A summary table for all the available single trial data (7 out of 8 cases) in the M135 correlation. The first column identifies the case, and the second column shows the average number of trials ($\bar{n}$) having high M135 correlation ($C_1 \geq 0.6$ and $C_2 \geq 1.0$) during the 500 ms long pre-stimulus interval. The next three columns summarize the M135 correlation during the M100 peak period (from 77 to 91 ms): the average number of trials having high M135 correlation ($\bar{n}_1$), the latency where the M100 correlation is at peak (t_1) and the number of high matching trials (n_1) at the latency of (t_1). Columns 6 to 8 summarize the M135 correlation during the M135 peak period (from 131 to 154 ms): the average number of high matching trials ($\bar{n}_2$), the latency where the number of high matching trials is maximum (T_2) and the maximum number of high matching trials (N_2), which are spilt into trials which have high M135 matching only and trials which have both high M100 and M135 matchings, as stated by the numbers in the bracket. Column 9 shows the total number of epochs (S_2), and in bracket the corresponding percentage, which, for at least one latency between T_2-5 and T_2+5 ms in each case, match the M135 average.

case label	pre-stm.	M100 period			M135 period			
	$\bar{n}$	$\bar{n}_1$	t_1(ms)	n_1	$\bar{n}_2$	T_2(ms)	N_2(o./b.)	S_2(%)
L-IPS-EO	14.7	0	83	0	36.6	144	43(20/23)	53(42)
L-IPS-EC	15.6	0	91	1	36.1	154	42(20/22)	51(41)
L-CON-EO	9.1	1.0	77	1	37.6	140	44(23/21)	62(50)
L-CON-EC	16.0	0.9	81	0	32.8	135	39(20/19)	47(38)
R-IPS-EO	6.3	0.8	89	0	10.1	146	17(14/2)	39(31)
R-IPS-EC	6.7	2.5	87	1	10.3	131	16(7/9)	53(42)
R-CON-EC	8.8	2.5	79	6	15.0	133	24(16/8)	50(40)

only, and how many epochs match well both the M100 and M135 average template. In the tables we also give the cumulative epoch numbers with high matching, i.e., the total number of epochs, showing a matching with the M100 or M135 average pattern, at some latency around the peak value, i.e., 60-100 ms for the M100. The population of epochs tends to divide in two, particularly on the left hemisphere, about 50% of the epochs match the average, which are divided in a ratio of 2:1 between those matching only the M100 and those matching both the M100 and M135. About one third of the trials show a matching with the M135 peak and they are equally divided between those only matching the M135 and those also matching the M100. The most striking feature of the tables is the reduction in matching of one component at the latency of the other. It is also worth noting that during the pre-stimulus interval more single trials behave like the M135 than the M100.

40-Hz studies

The correlation measures with spatiotemporal $\mathbf{V}_3$ templates was first applied to the filtered data in the 35-45 Hz band. On that occasion we have used the first 50 ms

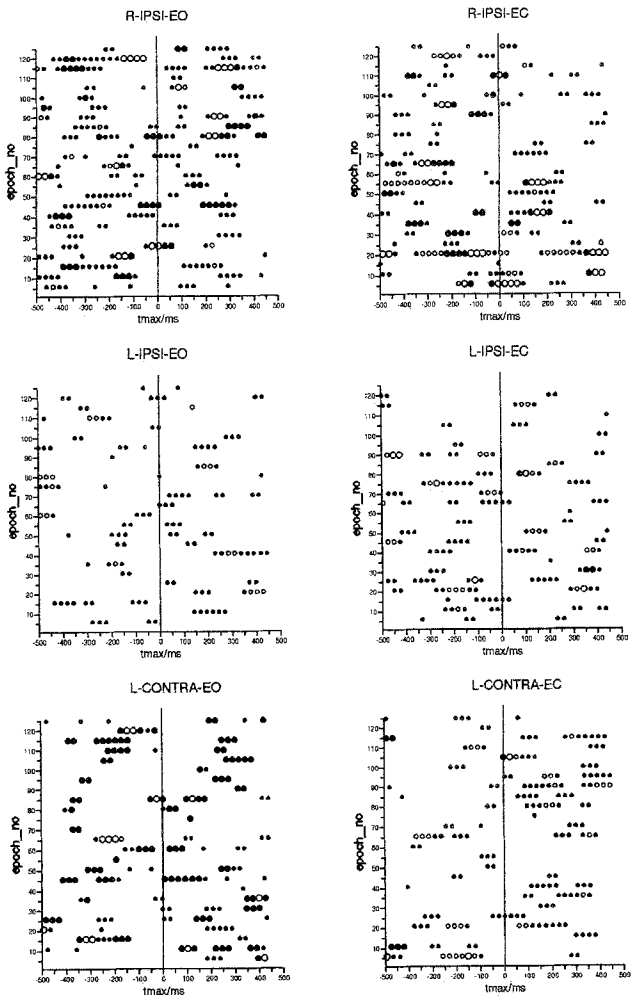

Figure 8. Epoch summary for the single trial signals in the 6 cases bandpass filtered in 35-45 Hz from -500 to 500 ms: an empty dot corresponds to $C_1 \geq 0.85$, and a filled dot corresponds to $0.7 \leq C_1 < 0.85$. The size of the dots indicates C_2, i.e., the big dots stand for $C_2 \geq 7.0$, and the small dots are for those $3.47 \leq C_2 < 7.0$. For avoiding clutter, every other 5th single trial is shown.

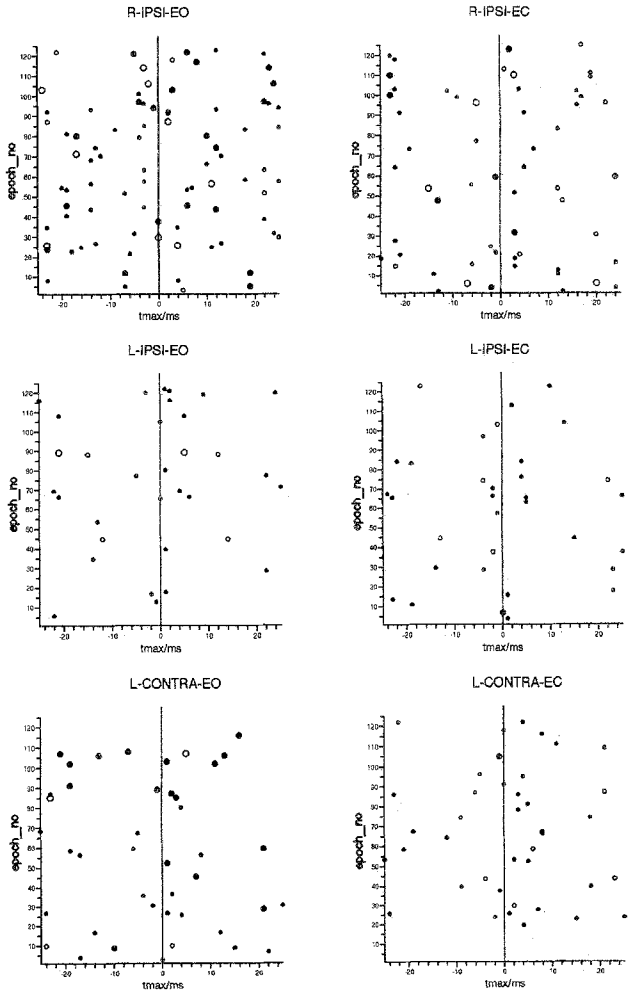

Figure 9. Epoch summary for the single trial signals in the 6 cases bandpass filtered in 35-45 Hz from -25 ms to 25 ms. All the epochs have high matching with the average between -25 and 25 ms are shown with the same display symbols defined in figure 8.

of the average signal as a target template and computed the two correlation measures for all single trials, again for 500 ms before to 500 ms after the onset of the stimulus (Liu 1995; Liu and Ioannides 1995). The 40-Hz oscillation identified in the first 50 ms of the average signal is matched in single trials, well before and well after stimulus onset. In figure 8, we use dot diagrams to show how widespread the 40-Hz oscillation is in time. In figure 9, we zoom in to the period around the onset of the stimulus to show when and how strongly the 40-Hz pattern identified in the average occurs in single trials. Note that in only a small number of trials a matching is observed with nearly zero phase lag with the average. Although the number of trials with high matching and zero phase lag with the average is small, typically 5-10% of all the single trials, it is higher than the matching occurring spontaneously and randomly throughout the period studied.

Discussion

The need to consider single trials has been recognised for a long time, but the notion that most of the signal in single trials is "brain noise" has prevailed. MEG analysis has adopted averaging for different reasons than EEG (Ioannides 1994a), but continued with its use when multichannel MEG probes made single trial analysis per-

fectly feasible. Even in EEG, processing of unaveraged signal is gaining ground (Haig et al. 1995; Liberati et al. 1992; Tomberg and Desmedt 1995). The main problem with single trial analysis of MEG signals is the computational burden incurred and the huge amount of output that such analysis produces. The $\mathbf{V}_3$ based methods we have described use spatial and temporal integrals and correlations together with the specificity of the $\mathbf{V}_3$ sensitivity to minimize the effect of random variations. They are designed to handle efficiently the computational burden associated with single trial analysis and they produce meaningful summaries of the results.

The MFT estimates for the average signal we are using in this study was compared with the equivalent current dipole (ECD) solution (Singh et al. 1994). In agreement with earlier similar studies (Ioannides et al. 1993a; Ioannides et al. 1993b), it was found that the MFT estimate and the ECD solution are in excellent agreement whenever the ECD solution fits the data very well. This usually is the case at the peaks of the average signal and particularly the M100 peak. In between the intervals where the ECD fits the data well, the ECD prediction varies widely and erratically in location; in contrast the MFT solution behaves in a much more stable manner showing a decline of activity in the areas seen at the main peaks and/or other areas becoming active as well. The excellent agreement between the MFT and the $\mathbf{V}_3$ maxima at the M100 peak, as evidenced in figure 4, allows us to be confident about the use of the $\mathbf{V}_3$ operator to provide specificity for focal nearby generators. By constructing the correlation estimator from the $\mathbf{V}_3$, integrated over a period of time and/or a region, we were able to extract reliable measures about how a specified pattern seen in the average signal is represented in the single trials. The $\mathbf{V}_3$ is for MEG, a vector operator analogous to the well known scalar operator of EEG, the Laplacian (Hjorth 1975); we are confident that our C_1 and C_2 correlation measures can be applied to EEG, by replacing the $\mathbf{V}_3$ with the Laplacian.

In most researchers' mind, the realization of single trial analysis was anticipated as an addition to the existing edifice, building on top of what the "safe, noise-free" average has established. The work we have discussed here and other work applying single trial analysis to pathological signal (Bamidis et al. 1995) has provided an explanation why some of the crudest models for the generators can be very successful in providing good descriptions of the average data and can even be used as markers of pathology (Rieke et al. 1995; Schwartz et al. 1995; Grummich et al. 1995). The MFT estimates extracted from unaveraged and minimally filtered MEG signals are highly variable from timeslice (ms) to timeslice (ms), as one would expect if the single trial signals are dominated by noise. A closer inspection of the MFT solutions points to a different conclusion. We have constructed instantaneous MFT solutions, and their integrals of intensity, with increasing integration time Δt, from 5 ms to 100 ms. We have compared corresponding MFT slices extracted from the average and its constituent single trials, and for the intensity distributions we have identified the order of activations of the main areas within each distribution (Liu 1995). If the single trial signal was dominated by noise, we should find no resemblance between the average and single trial MFT solutions. We find instead the same highly focal solutions in each case (Liu 1995; Ioannides et al. 1995b) but at different latencies in single trials, as long as Δt is small, particularly below 30 ms. As the integration time Δt increases the agreement improves dramatically and by 100 ms the areas identified and the order of activation become increasingly similar (Liu 1995; Ioannides et al. 1995b). The picture that emerges is not that of a rigid sequence, but of a range of temporal windows with trial to trial variability steadily decreasing as Δt increases. Within temporal windows of 30 ms or less we find little consistency in time (in the order of activations), although the same areas are identified in different trials, supporting the idea of a breakdown of time order at this temporal scale (Pöppel 1994). Even for $\Delta t \geq 100$ ms the order is not identical in each trial, but rather the trials are grouped into sets, each set accounting for a different sequence in the average. The $\mathbf{V}_3$ based correlation single trial analysis for the M100 and M135 peak further elaborates the same point, and strengthens the conclusion by allowing us to consider **all** single trials. In addition to the evident latency jitter, the analysis shows again that the features identified in the average need not be, and in all likelihood do not reflect a sequence of events.

In all the correlation studies for the 7 cases, we noticed that the number of matching epochs for the probe placed over the right hemisphere is slightly lower than the left hemisphere, 29-52 epochs out of 125 epochs (23%-42% of all epochs). The difference of the matching number between the left and right hemisphere can be due to a number of factors. All experiments with the probe over the right hemisphere were conducted first, 2 days before the experiments with the probe over the left hemisphere, so this may reflect some learning effect. More likely this is a reflection of the more tight within region organization on the left hemisphere, compared to the more between region connectivity on the right (Semmes 1968).

The 40 Hz work is intriguing, but in no way conclusive. The experiment we have used does not require much mental effort, nor does it involve a high level of attention, attributes which have been associated with increasing 40 Hz activity. The basic finding is however consistent with the work of Llinás and collaborators

(Ribary et al. 1991; Llinás and Ribary 1993; Joliot et al. 1994), suggesting that the processes associated with the generation of the 40 Hz signal occur spontaneously and intermittently as well as being reset in a subset of epochs by the introduction of the stimulus. The reset was found to be a rather rare event occurring in only a small fraction of epochs. Our results suggest that the increase in 40-Hz activity with cognitive load observed in some experiments (Tiitinen et al. 1993) is due to more trials participating in a fixed time lock sequence reset with the stimulus, rather than any increase in the 40-Hz intensity in individual single trials.

Our work does not resolve the recent controversy regarding the generation of the 40-Hz oscillation, but it provides some useful pointers. The thalamo-cortical origin of the gamma band activity advocated by Llinás (Llinás et al. 1994) was supported by an earlier MFT analysis of the early response (Ribary et al. 1991). The analysis reported here emphasizes deliberately the cortical contributions (the $\mathbf{V}_3$ operator reduces drastically the contribution from deep sources) so we can not address the question of deep generators directly. Franowicz and Barth (1995) observed in lightly anesthetized rats a 40-Hz response in the primary auditory cortex, with reduced activity at the onset of the stimulus and no evidence for deep activity. Llinás has shown that 40-Hz oscillation is related to the state of the subject (Llinás and Ribary 1993; Llinás and Pare 1991), namely, the 40-Hz is not seen in delta sleep but it is present in the awake state and REM sleep, and the reset of the 40-Hz is absent in all stages of sleep. The Franowicz observations (Franowicz and Barth 1995) were made on lightly anesthetized preparations, while the human observations were made when the subject was awake, alert and focusing on a demanding task (Joliot et al. 1994). Galambos has shown many years ago that the classical auditory path remains active in anesthetized cats (Galambos et al. 1961), but another more medial pathway must be involved in awake animals. It is likely that the thalamo-cortical oscillations may involve this second pathway, while the purely cortical events in the primary auditory cortex the classical route. The best way of examining these questions is through the design of experiments, where not only the physical properties of the stimulus are varied, but also the subject's response and perception of the stimulus properties and significance are recorded in every single trial.

In conclusion, we have demonstrated that the analysis of single trial MEG data is perfectly feasible. Although our primary aim was to develop a methodology capable of tackling single trial data, the application of the tools we have developed to rather innocuous auditory evoked fields has provided powerful hints about cortical processing. Our results cast doubt on the idea that the analysis of the average MEG or EEG signal relate directly to the temporal dynamics of brain processes. The most parsimonious explanation of our results is that the average is a superposition of histories each reflected in different subsets of the epochs. Alternative explanations could be made along the lines suggested by Galambos (Galambos 1995), i.e., a more holistic activation following the onset of the stimulus with oscillations spanning many brain centers in competing networks. Different subsets of epochs could correspond to different networks or different "response modes" of the same network. Whatever the explanation the warning is clear: the early imposition of constraints either in time (e.g., unnecessary filtering) or on the basis of anatomy (Fuchs et al. 1995) may eliminate significant information. The use of averaging is very effective in eliminating noise, but it also eliminates information and makes the interpretation of results difficult; this is especially relevant to the many recent studies using either fMRI (Simpson et al. 1995) or PET (Snyder et al. 1995) loci of activity to constrain EEG and/or MEG solutions. We repeat the advice earlier given (Ioannides et al. 1995a): at this stage of functional brain imaging, it is wise, in EEG and MEG studies, to impose as few prior constraints as necessary so that we can test the solutions against anatomical reality rather than impose constraints which make interpretation difficult. Given how much information is lost by averaging and heavy filtering, any agreement or consistency between fMRI and average EEG or MEG reveals less about dynamics and more about the limitations of heamodynamic measures!

References

Ahonen, A.I., Hämälainen, M.S., Kajola, M.J., Knuutila, J.E., Laine, P.L., Lounasmaa, O.V., and et al. A 122-channel Magnetometer Covering the Whole Head. In: A. Dittmar and J.C. Froment (Ed.), Proceedings of the Satellite Symposium on Neuroscience and Technology, 14th Annual International Conference of the IEEE Engineering in Medicine and Biology Society. IEEE Engineering and Medicine and Biology Society, Lyon, France, Nov. 1992: 16-20.

Basar, E., Basar-Eroglu, C., Röschke, J. and Schütt, A. The EEG is a Quasi-deterministic Signal Anticipating Sensory-Cognitive Tasks. In: E. Basar, and T.H. Bullock (Ed.), Brain Dynamics. Springer-Verlag Berlin Heidelberg, 1989: 43-71.

Bamidis, P.D., Hellstrand, E., Lidholm, H., Abraham-Fuchs, K., and Ioannides, A.A. MFT in Complex Partial Epilepsy: Spatial-temporal Estimates of Interictal Activity. Neuroreport, 1995, 7(1): 17-23.

Desimone, R., Albright, T.D., Gross, C.G. and Bruce, C. Stimulus-selective Properties of Inferior Temporal Neurons in the Macaque. J. Neurosc., 1984, 4: 2051-2062.

Franowicz, M.N., and Barth, D.S. Comparison of Evoked Potentials and High-Frequency (Gamma-Band) Oscillating Potentials in Rat Auditory Cortex. Journal of Neurophysiology, 1995, 74: 96-111.

Fuchs, M., Wagner, M., Wischmann, H.A., and Dössel, O. Cor-

tical Current Imaging by Morphologically Constrained Reconstructions. In: C. Baumgartner, L. Deeke, G. Stroink and S.J. Williamson (Ed.), Biomagnetism: Fundamental Research and Clinical Applications, Elsevier Science Publishers, Amsterdam, 1995: 320-325.

Galambos, R., Myers, R.E., and Sheatz, G.C. Extralemniscal Activation of Auditory Cortex in Cats. The American Journal of Physiology, 1961, 200(1): 23-28.

Galambos, R. EPIC X: Past, Present, Future. In: G. Karmos, M. Molnár, V. Csépe, I. Czigler and J.E. Desmedt (Ed.), Perspectives of Event-Related Potentials Research (EEG Suppl. 44). Elsevier Science Publishers, Amsterdam, 1995: 3-20.

Grimes, D.I.F., Lennard, R.F. and Swithenby, S.J. Macroscopic Ionic Currents within the Human Leg. Phys. Med. Biol., 1985, 30(10): 1101-1112.

Grimes, D.I.F. and Ioannides, A.A. Reconstructing 3-dimensional Line Current Sources from Magnetic Field Data.In: K. Atsumi, M. Kotani, S. Ueno, T. Katila, and S.J. Williamson (Ed.), Biomagnetism 87. Tokyo Denki University Press, 1988: 134-137.

Grummich, P., Vieth, J., Kober, H., Pongratz, H., Ulbricht, D., and Ganslandt, O. Localization of Focal Spontaneous Beta Wave Activity Associated with Structural Lesions in the Brain. In: C. Baumgartner, L. Deeke, G. Stroink and S.J. Williamson (Ed.), Biomagnetism: Fundamental Research and Clinical Applications. Elsevier Science Publishers, Amsterdam, 1995: 75-79.

Haig, A.R., Gordon, E., Rogers, G. and Anderson, J. Classification of Single-trial ERP Sub-types: Application of Globally Optimal Vector Quantization using Simulated Annealing. Electroenceph. Clin. Neurophysiol., 1995, 94: 288-297.

Hämälainen, M.S., Hari, R., Ilmoniemi, R.J., Knuutila, J. and Lounasmaa, O.V. Magnetoencephalography - Theory, Instrumentation, and Applications to Noninvasive Studies of the Working Human Brain. Reviews of Modern Physics, 1993, 65(2): 413-497.

Hjorth, B. An On-line Transformation of EEG Scalp Potentials into Orthogonal Source Derivations. Electroenceph. Clin. Neurophysiol., 1975, 39: 526-530.

Hosaka, H. and Cohen, D. Visual Determination of Generators of the Magnetocardiogram. J. Electrocardiology, 1976, 9: 426-432.

Hubel, D.H., and Wiesel, T.N. Receptive Fields, Binocular Interaction and Functional Architectures of the Cat's Visual Cortex. J. Physiol., 1962, 160:106-154.

Ioannides, A.A. Graphical Solutions and Representations for the Biomagnetic Inverse Problem. In: P.C. Sabatier (Ed.), Advances in Electronics and Electron Physics Supplement 19, Inverse Problems: an Interdisciplinary Study. Academic press, Orlando, 1987: 205-216.

Ioannides, A.A., Bolton, J.P.R. and Clarke, C.J.S. Continuous Probabilistic Solutions to the Biomagnetic Inverse Problem. Inverse Problem, 1990a, 6: 523-542.

Ioannides, A.A., Hasson, R. and Miseldine, G.J. Model-dependent Noise Elimination and Distributed Source Solutions for the Biomagnetic Inverse Problem. In: A.F. Gmitro and etal. (Ed.), Digital Image Synthesis and Inverse Optics, 1990b, Proc. SPIE 1351: 471-481.

Ioannides, A.A., Hellstrand, E., and Abraham-Fuchs, K. Point and Distributed Current Density Analysis of Interictal Epileptic Activity Recorded by Magnetoencephalography. Physiological Measurements, 1993a, 14: 121-130.

Ioannides, A.A., Singh, K.D., Hasson, R., Baumann, S.B., Rogers, R.L., Guinto, F.C. and Papanicolaou, A.C. Comparison of Current Dipole and Magnetic Field Tomography Analyses of the Cortical Response to Auditory Stimuli. Brain Topography, 1993b, 6: 27-34.

Ioannides, A.A. Searchlights into the Brain. The Open University (U.K.) video, August 1993.

Ioannides, A.A. Estimates of Brain Activity using Magnetic Field Tomography and Large Scale Communication within the Brain. In: M.W. Ho, F.A. Popp, and U. Warnke (Ed.), Bioelectrodynamics and Biocommunication. World Scientific, Singapore, 1994a: 319-353.

Ioannides, A.A. Estimates of 3D Brain Activity ms by ms from Biomagnetic Signals: Method (MFT), Results and their Significance. In: E. Eiselt, U. Zwiener, and H. Witte (Ed.), Quantitative and Topological EEG and MEG Analysis. Universitätsverlag Druckhaus-Maayer GmbH, Jena, 1994b: 59-68.

Ioannides, A.A., Stephan, K.M., Fenwick, P.B.C., Lumsden, J., Fenton, G.W., Liu, M.J., Vieth, J., Squires, K.C., Lawson, D., Myers, R., Fink, G.R. and Frackowiak, R.S.J. Analysis of MEG Signals from a GO/NOGO Avoidance Paradigm and Comparison of Estimates of Brain Activity using PET. In: C. Baumgartner, L. Deeke, G. Stroink, and S.J. Williamson (Ed.), Biomagnetism: Fundamental Research and Clinical Applications. Elsevier Science Publishers, Amsterdam, 1995a: 262-265.

Ioannides, A.A., Liu, M.J., Liu, L.C., Bamidis, P.D., Hellstrand, E. and Stephan, K.M. Magnetic Field Tomography of Cortical and Deep Processes: Examples of "Real-Time Mapping" of Averaged and Single Trial MEG Signals. International Journal of Psychophysiology, 1995b, 20(3): 161-175.

Joliot, M., Ribary, U. and Llinás, R. Human Oscillatory Brain Activity near 40 Hz Coexists with Cognitive Temporal Binding. Proc. Natl. Acad. Sci. USA, 1994, 91: 11748-11751.

Liberati, D., DiCorrado, S. and Mandelli, S. Topographic Mapping of Single Sweep Evoked Potentials in the Brain. IEEE Transactions on Biomedical Engineering, 1992, 39(9): 943-951.

Liu, L.C. and Ioannides, A.A. Single Epoch Analysis of MEG Signals. In: C. Baumgartner, L. Deeke, G. Stroink, and S.J. Williamson (Ed.), Biomagnetism: Fundamental Research and Clinical Applications. Elsevier Science Publishers, Amsterdam, 1995: 439-444.

Liu, L.C. Single Epoch Analysis and Bi-hemispheric Study of Magnetoencephalographic (MEG) Signals using Vector Signal Transformation $\mathbf{V}_3$ and Magnetic Field Tomography (MFT). PhD thesis, Department of Physics, The Open University, U.K., February 1995.

Liu, M.J., Hasson, R. and Ioannides, A.A. A Transputer-based System for Magnetic Field Tomography. In R. Grebe, J. Hektor, S.C. Hilton, M. Jane, and P.H. Welch (Ed.), Transputer Applications and Systems'93. IOS Press, Amsterdam, 1993, 2: 1290-1297.

Llinás, R. and Pare, D. Commentary of Dreaming and Wakefulness. Neuroscience, 1991, 44: 521-535.

Llinás, R. and Ribary, U. Coherent 40-Hz Oscillation Characterizes Dream State in Humans. Proc. Natl. Acad. Sci. USA, 1993, 90: 2078-2081.

Llinás, R., Ribary, U., Joliot, M., and Wang, X.J. Content and Context in Temporal Thalamo-cortical Binding. In: G. Buzsáki and etal. (Ed.), Temporal Coding in the Brain. Spring-Varlag Berlin Heidelberg, 1994: 251-272.

Lütkenhöner , B., Pantev, C., Grunwald, A., and Menninghaus, E. Source-space Projection of Single Trials of the Auditory Evoked Field. In: C. Baumgartner, L. Deeke, G. Stroink, and S.J. Williamson (Ed.), Biomagnetism: Fundamental Research and Clinical Applications, Elsevier Science Publishers, Amsterdam, 1995: 347-351.

Mitzdorf, U., Li, B.H. and Pöppel, E. Mass-action View of Single-cell Responses to Stimulation of the Receptive Field and/or beyond: Exemplification with Data from the Rabbit Primary Visual Cortex. Electroenceph. Clin. Neurophysiol., 1994, 92: 442-455.

Nicolelis, M.A., Baccala, L.A., Lin, R.C., and Chapin, J.K. Sensorimotor Encoding by Synchronous Neural Ensemble Activity at Multiple Levels of the Somatosensory System. Science, 1995, 268: 1353-1358.

O'Keefe, J. and Recce, M.L. Phase Relationship between Hippocampal Place Units and the EEG Theta Rhythm. Hippocampus, 1993, 3: 317-330.

Pöppel, E. Temporal Mechanisms in Perception. International Review of Neurobiology, 1994, 37: 185-202.

Ribary, U., Ioannides, A.A., Singh, K.D., Hasson, R., Bolton, J.P.R., Lado, F., Mogilner, A., and Llinás,R. Magnetic Field Tomography (MFT) of Coherent Thalamo-Cortical 40 Hz Oscillations in Humans. Proc. Natl. Acad. Sci. USA, 1991, 88: 11037-11041.

Rieke, K., Gallen, C.C., Sobel, D.F., Otis, S., Bernstein, E., Schwartz, B., and Hirschkoff, E. Magnetic Source Imaging in Cerebrovascular Diseases. In: C. Baumgartner, L. Deeke, G. Stroink and S.J. Williamson (Ed.), Biomagnetism: Fundamental Research and Clinical Applications. Elsevier Science Publishers, Amsterdam, 1995: 46-49.

Schwartz, B.J., Gallen, C.C., Aung, M., Sobel, D.F., Hirschkoff, E.C., and Bloom, F.E. Magnetoencephalographic Detection of Focal Slowing Associated with Head Trauma. In: C. Baumgartner, L. Deeke, G. Stroink, and S.J. Williamson (Ed.), Biomagnetism: Fundamental Research and Clinical Applications. Elsevier Science Publishers, Amsterdam, 1995: 66-69.

Semmes, J. Hemispheric Specialization: A Possible Clue to Mechanism. Neurophysiologia, 1968, 6: 11-26.

Simpson, G.V., Pflieger, M.E., Foxe, J.J., Ahlfors, S.P., Vaughan, H.G., Hrabe, J., Ilmoniemi, R.J. and Lantos, G. Dynamic Neuroimaging of Brain Function. J. Clin. Neurophysiol., 1995, 12(5): 432-449.

Singh, K.D., Ioannides, A.A., Gray, N., Kober, H., Pongratz, H., Daun, A., Grummich, P. and Vieth, J. Distributed Current Analyses of Bi-hemispheric Magnetic N1m Responses to Ipsi/Contralateral Monaural Stimulus from a Single Subject. Electroenceph. Clin. Neurophysiol., 1994, 92: 365-368.

Snyder, A.Z., Abdullaev, Y.G., Posner, M.I. and Raichle, M.E. Scalp Electrical Potentials Reflect Regional Cerebral Blood Flow Responses during Processing of Written Words. Proc. Natl. Acad. Sci. USA, 1995, 92: 1689-1693.

Tiitinen, H., Sinkkonen, J., Reinikainen, K., Alho, K., Lavikainen, J., and Näätänen, R. Selective Attention Enhances the Auditory 40-Hz Transient Response in Humans. Nature, 1993, 364: 59-60.

Tomberg, C. and Desmedt, J.E. A Method for Identifying Short-Latency Human Cognitive Potentials in Single Trials by Scalp Mapping. Neuroscience Letters, 1995, 168: 123-125.

Vaadia, E., Haalman, I., Abeles, M., Bergman, H., Prut, Y., Slovin, H., and Aertsen, A. Dynamics of Neuronal Interactions in Monkey Cortex in Relation to Behavioural Events. Nature, 1995, 373: 515-518.